JOURNAL OF THE AMERICAN CHEMICAL SOCIETY

Article

Ir(ethene): Metal or Carbon Radical?

Dennis G. H. Hetterscheid, Jasper Kaiser, Eduard Reijerse, Theo P. J. Peters, Simone Thewissen, Arno N. J. Blok, Jan M. M. Smits, Ren de Gelder, and Bas de Bruin

J. Am. Chem. Soc., **2005**, 127 (6), 1895-1905• DOI: 10.1021/ja0439470 • Publication Date (Web): 22 January 2005

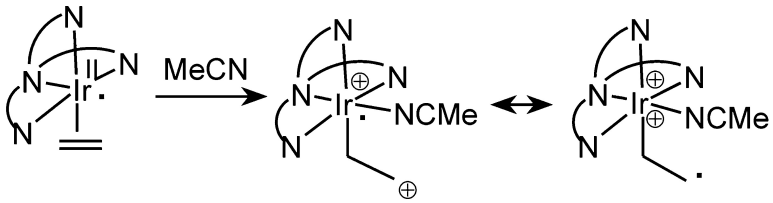

More About This Article

Additional resources and features associated with this article are available within the HTML version:

- Supporting Information
- Links to the 9 articles that cite this article, as of the time of this article download
- Access to high resolution figures
- Links to articles and content related to this article
- Copyright permission to reproduce figures and/or text from this article

View the Full Text HTML

J|A|C|S
ARTICLES
Published on Web 01/22/2005

Ir^{II}(ethene): Metal or Carbon Radical?

Dennis G. H. Hetterscheid,† Jasper Kaiser,† Eduard Reijerse,‡ Theo P. J. Peters,† Simone Thewissen,† Arno N. J. Blok,† Jan M. M. Smits,† René de Gelder,† and Bas de Bruin*,†

Contribution from the Radboud University Nijmegen, Institute for Molecules and Materials, Department of Metal-Organic Chemistry, Toernooiveld 1, NL-6525 ED Nijmegen (The Netherlands), Max-Planck-Institut für Bioanorganische Chemie, Stiftstrasse 34-36, D-45470 Mülheim an der Ruhr (Germany)

Received October 5, 2004; E-mail: B.deBruin@science.ru.nl

Abstract: One-electron oxidation of $[(Me_n tpa)Ir^{I}(ethene)]^{+}$ complexes (Me_3tpa = *N,N,N*-tri(6-methyl-2-pyridylmethyl)amine; Me_2tpa = *N*-(2-pyridylmethyl)-*N,N,*-di[(6-methyl-2-pyridyl)methyl]-amine) results in relatively stable, five-coordinate Ir^{II}−olefin species $[(Me_n tpa)Ir^{II}(ethene)]^{2+}$ ($\mathbf{1}^{2+}$: $n = 3$; $\mathbf{2}^{2+}$: $n = 2$). These contain a "vacant site" at iridium and a "non-innocent" ethene fragment, allowing radical type addition reactions at both the metal and the ethene ligand. The balance between metal- and ligand-centered radical behavior is influenced by the donor capacity of the solvent. In weakly coordinating solvents, $\mathbf{1}^{2+}$ and $\mathbf{2}^{2+}$ behave as moderately reactive metallo-radicals. Radical coupling of $\mathbf{1}^{2+}$ with NO in acetone occurs *at the metal*, resulting in dissociation of ethene and formation of the stable nitrosyl complex $[(Me_3tpa)Ir(NO)]^{2+}$ ($\mathbf{6}^{2+}$). In the coordinating solvent MeCN, $\mathbf{1}^{2+}$ generates more reactive radicals; $[(Me_3tpa)Ir(MeCN)(ethene)]^{2+}$ ($\mathbf{9}^{2+}$) by MeCN coordination, and $[(Me_3tpa)Ir^{II}(MeCN)]^{2+}$ ($\mathbf{10}^{2+}$) by substitution of MeCN for ethene. Complex $\mathbf{10}^{2+}$ is a metallo-radical, like $\mathbf{1}^{2+}$ but more reactive. DFT calculations indicate that $\mathbf{9}^{2+}$ is intermediate between the slipped-olefin $Ir^{II}(CH_2{=}CH_2)$ and ethyl radical $Ir^{III}-CH_2-CH_2{\bullet}$ resonance structures, of which the latter prevails. The ethyl radical character of $\mathbf{9}^{2+}$ allows radical type addition reactions *at the ethene ligand*. Complex $\mathbf{2}^{2+}$ behaves similarly in MeCN. In the absence of further reagents, $\mathbf{1}^{2+}$ and $\mathbf{2}^{2+}$ convert to the ethylene bridged species $[(Me_n tpa)(MeCN)Ir^{III}(\mu_2\text{-}C_2H_4)Ir^{III}(MeCN)(Me_3tpa)]^{4+}$ ($n = 3$: $\mathbf{3}^{4+}$; $n = 2$: $\mathbf{4}^{4+}$) in MeCN. In the presence of TEMPO (2,2,6,6-tetramethyl-1-piperidinyloxo), formation of $\mathbf{3}^{4+}$ from $\mathbf{1}^{2+}$ in MeCN is completely suppressed and only $[(Me_3tpa)Ir^{III}(TEMPO^{-})(MeCN)]^{2+}$ ($\mathbf{7}^{2+}$) is formed. This is thought to proceed via radical coupling of TEMPO *at the metal center* of $\mathbf{10}^{2+}$. In the presence of water, hydrolysis of the coordinated acetonitrile fragment of $\mathbf{7}^{2+}$ results in the acetamido complex $[(Me_3tpa)Ir^{III}(NHC(O)CH_3))$-$(TEMPO\mathit{H})]^{2+}$ ($\mathbf{8}^{2+}$).

Introduction

Metallo-enzyme reactions frequently involve open-shell paramagnetic species. Their reactivity is not fully understood, but it is clear that besides the metal, ligand radicals can play an important role as well. This especially holds for oxygenating enzymes, like cytochrome P450,[1] galactose oxidase,[2] and molybdenum enzymes.[3] Ligand oxidation does not only lead to stabilization of unusually high formal oxidation states of the metal, but also to true ligand radical reactivity in the key steps of the reaction mechanisms. For galactose oxidase, both metallo- and ligand-radical reactivity is needed to account for the mechanism of alcohol oxidation.[2] Radicals also play an important role in the mechanisms of many synthetic oxygenating catalysts. As in biology, this encompasses both the concept of 'ligand non-innocence',[4] and true ligand radical reactivity. The role of radical-type reactions in metal-assisted oxygenation reactions by enzymes, their model systems and by synthetic oxygenation catalysts has been reviewed recently.[1c]

Traditionally, most catalytic reactions mediated by *organometallic* complexes proceed via closed-shell species. Their catalytic pathways proceed via two-electron reaction steps (e.g., oxidative addition, reductive elimination, β-hydrogen elimination and migratory insertion/de-insertion). Radical-type reactivity of open-shell organometallic complexes is still a largely uncharted research area, although increasing reports on the involvement of organometallic radicals in catalysis has stimulated interest in the properties of these species.[5]

Organometallic radicals are mostly low-spin 17- or 19-VE (valence electron) species with the unpaired spin-density located

† Radboud University Nijmegen, Institute for Molecules and Materials, Department of Metal-Organic Chemistry.
‡ Max-Planck-Institut für Bioanorganische Chemie.

(1) (a) Collman, J. P.; Boulatov, R.; Sunderland, C. J.; Fu, L. *Chem. Rev.* **2004**, *104*, 561. (b) Kim, E.; Chufán, E. E.; Kamaraj, K.; Karlin, K. D. *Chem. Rev.* 2004, *104*, 1077. (c) Limberg, C. Angew. Chem., Int. Ed. 2003, *42*, 5932.
(2) Costas, M.; Mehn, M. P.; Jensen, M. P.; Que, L., Jr. *Chem. Rev.* **2004**, 104, 939.
(3) Enemark, J. H.; Cooney, J. J. A. *Chem. Rev.* **2004**, *104*, 1175.
(4) See, for example: (a) Blanchard, S.; Bill, E.; Weyhermüller, T.; Wieghardt, K. *Inorg. Chem.* **2004**, *43*, 2324. (b) Min, K. S.; Weyhermüller, T.; Wieghardt, K. *Dalton Trans.* 2004, 178. (c) Chun, H.; Bill, E.; Weyhermüller, T.; Wieghardt, K. *Inorg. Chem.* 2003, *42*, 5612. (d) Ray, K.; Weyhermüller, T.; Goossens, A.; Craje, M. W. J.; Wieghardt, K. *Inorg. Chem.* 2003, *42*, 4082. (e) Knijnenburg, Q.; Hetterscheid, D.; Kooistra, T. M.; Budzelaar, P. H. M. *Eur. J. Inorg. Chem.* 2004, *6*, 1204.

Scheme 1. 'Ligand Non-innocence' in Open-Shell Transition Metal Olefin Complexes

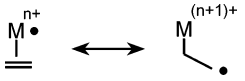

at the metal. This explains that most of these species reveal metallo-radical reactivity, like halogen atom abstraction, hydrogen abstraction and capture of other radicals by the metal (which includes dimerization by formation of metal−metal bonds).[6] For complexes containing π-accepting ligands such as CO and olefins, an alternative description is possible, in which the unpaired electron resides *at the ligand*, leaving the metal in the usual 16- or 18-VE closed-shell configuration (Scheme 1).[7] This is similar to the concept of 'ligand non-innocence' in coordination and bio-inorganic chemistry. For such species one might expect ligand-centered radical reactivity. This is rarely observed, but the few known examples have been reviewed, and reveal interesting reaction pathways.[5,6] Most related to the chemistry in this paper are organometallic *olefin* complexes revealing such ligand radical behavior. Examples involve ligand-ligand radical coupling,[8] metal−ligand radical coupling[9] and allylic hydrogen abstraction reactions,[10] demonstrating the possibility of new reaction pathways for olefin activation, very different from those of traditional organometallic chemistry. Most of these examples concern olefin complexes of low-spin Co, Rh, and Ir metallo-radical species in the formal oxidation states 0 or +II. Only a few stable open-shell olefin complexes of the Co-triad are known.[5h,10c,11,12] The above reactive ones could not be isolated, and their ligand centered radical behavior could only be inferred from the reaction products from in situ generated species. To our knowledge, only one stable mononuclear Ir^{II}−olefin complex has been reported, viz. $[(C_6Cl_5)_2Ir^{II}(cod)]$ (cod = *Z,Z*-1,5-cyclooctadiene).[15c] Mononuclear M^{II} (M = Rh, Ir) and M^0 (M = Co, Rh, Ir) complexes are generally rare, even without olefin ligands.[13−15] Low-spin cobalt(II) species are more common, but these are also known to reveal radical type behavior.[16]

Scheme 2. Synthesis of $\mathbf{1}^{2+}$ and $\mathbf{2}^{2+}$

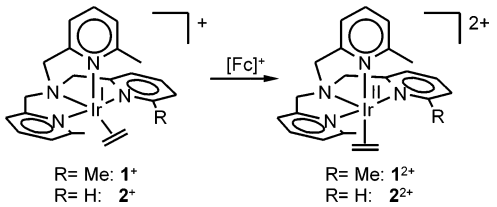

We here describe the synthesis and characterization of new open-shell organometallic olefin species $[(Me_n tpa)Ir^{II}(ethene)]^{2+}$ (n = 2, 3), which are the first examples of stable Ir^{II}(ethene) species. Although these are stable by themselves, they can be triggered to undergo radical-type reactions by addition of donor-reagents. This constitutes a new approach for tuning the reactivity of open-shell metal-olefin complexes. In this paper, we will describe the reactivity of these species toward closed-shell and open-shell reagents, and we will rationalize the observations through mechanisms involving both metallo-radical and ethene ligand-centered radical behavior. Part of this work has been communicated.[17]

2. Results and Discussion

2.1 Synthesis and Characterization of N_4-Ligand Ir^{II}-(ethene) Complexes. The iridium(II) complexes $[(Me_3tpa)Ir^{II}(ethene)](PF_6)_2$ ($\mathbf{1}(PF_6)_2$) (Me_3tpa = *N,N,N*-tri(6-methyl-2-pyridylmethyl)amine) and $[(Me_2tpa)Ir^{II}(ethene)](PF_6)_2$ ($\mathbf{2}(PF_6)_2$) (Me_2tpa = *N*-(2-pyridylmethyl)-*N,N-di*-(6-methyl-2-pyridylmethyl)-amine) were obtained as dark brown precipitates by chemical oxidation of the corresponding iridium(I) complexes $\mathbf{1}(PF_6)$ and $\mathbf{2}(PF_6)$ [17b,18] with ferrocenium hexafluorophosphate ($Fc(PF_6)$) in dichloromethane (Scheme 2).

Both $\mathbf{1}^{2+}$ and $\mathbf{2}^{2+}$ are reasonably stable in the weakly coordinating solvent acetone. Complex $\mathbf{1}^{2+}$ is stable for at least 48 h. A slight degradation of $\mathbf{2}^{2+}$ was observed after 2 h at

(5) (a) Astruc, D. *Electron-Transfer and Radical Processes in Transition-Metal Chemistry*; VCH: New York, 1995. (b) Baird, M. C. *Chem. Rev.* **1988**, *88*, 1217. (c) Trogler, W. C., Ed.; Organometallic Radical Processes, Journal of Organometallic Chemistry Library, vol. 22, Elsevier: Amsterdam, 1990. (d) Connelly, N. G. *Chem. Soc. Rev.* **1989**, *18*, 153. (e) Channon, M., Julliard, M., Poite, J. C., Eds.; Paramagnetic organometallic Species in Activation/Selectivity, catalysis, NATO ASI series, Kluwer Academic: Dordrecht, 1987. (f) MacAdams, L. A.; Buffone, G. P.; Incarvito, C. D.; Golen, J. A.; Rheingold, A. L.; Theopold, K. H. *Chem. Commun.* **2003**, *10*, 1164−1165. (g) Pariya, C.; Theopold, K. H. *Current Science* **2000**, *78*(11), 1345−1351. (h) Jewson, J. D.; Liable-Sands, L. M., Yap, G. P. A.; Rheingold, A. L.; Theopold, K. H. *Organometallics* **1999**, *18*, 300−305. (i) Poli, R. *Chem. Rev.* **1996**, *96*, 2135−2204.

(6) Toracca, K. E.; McElwee-White, L.*Coord. Chem. Rev.* **2000**, *206−207*, 469.

(7) Tyler, D. R. *Acc. Chem. Res.* **1991**, *24*, 325.

(8) a) Geiger, W. E.; Genett, T.; Lane, G. A.; Salzer, A. L.; Rheingold, A. L.*Organometallics* **1986**, *5*, 1352. (b) Ernst, R. D.; Ma, H.; Sergeson, G.; Zahn, T.; Ziegler, M. L. *Organometallics* **1987**, *6*, 848. (c) Newbound, T. D.; Arif, A. M.; Wilson, D. R.; Rheingold, A. L.; Ernst, R. D. *J. Organomet. Chem.* **1992**, *435*, 73. (d) Zou, C. F.; Ahmed, K. J.; Wrighton, M. S. *J. Am. Chem. Soc.* **1989**, *111*, 1133. (e) Novikova, L. N.; Mazurchik, B. A.; Ustynyuk, N. A.; Opruneko, Y. F.; Rochev, V. Y.; Bekeshev, V. G. *J. Organomet. Chem.* **1995**, *498*, 25. (f) Brammer, L.; Connelly, N. G.; Edwin, J.; Geiger, W. E.; Orpen, A. G.; Sheridan, J. B. *Organometallics* **1988**, *7*, 1259. (g) Bunn, A.; Wayland, B. B. *J. Am. Chem. Soc.* **1992**, *114*, 6917−6919, and references therein.

(9) Wayland, B. B.; Sherry, A. E.; Bunn, A. G. *J. Am. Chem. Soc.* **1993**, *115*, 7675, and references therein.

(10) (a) Orsini, J.; Geiger, W. E. *J. Electroanal. Chem.* **1995**, *380*, 83. (b) Burrows, A. D.; Green, M.; Jeffery, J. C.; Lynam, J. M.; Mahon, M. F. *Angew. Chem., Int. Ed. Engl.* **1999**, *38*, 3043. (c) Hetterscheid, D. G. H.; de Bruin, B.; Smits, J. M. M.; Gal, A. W. *Organometallics* **2003**, *22*, 3022−3024.

(11) Rh^{II}−olefin complexes: (a) Casado, M. A.; Pérez-Torrente, J. J.; López, J. A.; Ciriano, M. A.; Alonso, P. J.; Lahoz, F. J.; Oro, L. A. *Inorg. Chem.* **2001**, *40*, 4785. (b) Shaw, M. J.; Geiger, W. E.; Hyde, J.; White, C. *Organometallics* **1998**, *17*, 5486. (c) Carcia, M. P.; Jimenez, M. V.; Cuesta, A.; Siurana, C.; Oro, L. A.; Lahoz, F. J.; Lopez, J. A.; Catalan, M. P.; Tiripicchio, A.; Lanfranchi, M. *Organometallics* **1993**, *12*, 3257. (d) Hetterscheid, D. G. H.; Smits, J. M. M.; de Bruin, B. *Organometallics* **2004**, *23*, 4236−4246.

(12) Ir^{II}−olefin complexes: (a) Garcia, M. P.; Jimenez, M. V.; Oro, L. A.; Lahoz, F. J.; Alonso, P. J. *Angew. Chem., Int. Ed. Engl.* **1992**, *31*, 1527. (b) see ref (17).

(13) Oxidation state 0 complexes of Co, Rh and Ir: (a) Deblon, S.; Liesum, L.; Harmer, J.; Schonberg, H.; Schweiger, A.; Grutzmacher, H. *Chem. Eur. J.* **2002**, *8*(3), 601, and references therein.

(14) For an overview of Rh^{II} and Ir^{II} complexes and their reactivity, see: (a) DeWit, D. G. *Coord. Chem. Rev.* **1996**, *147*, 209−246. (b) Pandey, K. K. *Coord. Chem. Rev.* **1992**, *121*, 1−42.

(15) For recent examples of mononuclear iridium(II) complexes, see: (a) Zhai, H. L.; Bunn, A.; Wayland, B. B. *Chem. Commun.* **2001**, 1294−1295; (b) Collman, J. P.; Chang, L. L.; Tyvoll, D. A. *Inorg. Chem.* **1995**, *34*, 1311−1324. (c) Garcia, M. P.; Jimenez, M. V.; Oro, L. A.; Lahoz, F. J.; Alonso, P. J. *Angew. Chem., Int. Ed. Engl.* **1992**, *31*, 1527−1529. (d) Garcia, M. P.; Jimenez, M. V.; Oro, L. A.; Lahoz, F. J.; Tiripicchio, M. C.; Tiripicchio, A. *Organometallics* **1993**, *12*, 4660−4663. (e) Bond, A. M.; Humphrey, D. G.; Menglet, D.; Lazarev, G. G.; Dickson, R. S.; Vu, T. *Inorg. Chim. Acta* **2000**, *300*, 565−571. (f) Danopoulos, A. A.; Wilkinson, G.; Hussainbates, B.; Hursthouse, M. B. *J. Chem. Soc., Dalton Trans.* **1992**, 3165−3170.

(16) Griffith, W. P.; Wilkinson, G. *J. Chem. Soc.* **1959**, 2757. (b) Burnett, M. G.; Connolly, P. J.; Kemball, C. *J. Chem. Soc. A* **1967**, 800. (c) Reger, D. L.; Habib, M. M.; Fauth, D. J. *Tetrahedron Lett.* **1979**, *2*, 115, and references therein.

(17) (a) de Bruin, B.; Peters, T. P. J.; Thewissen, S.; Blok, A. N. J.; Wilting, J. B. M.; de Gelder, R.; Smits, J. M. M.; Gal, A. W. *Angew. Chem., Int. Ed.* **2002**, *41*(12), 2135−2138. (b) de Bruin, B.; Thewissen, S.; Yuen, T.-W.; Peters, T. P. J.; Smits, J. M. M.; Gal, A. W. *Organometallics* **2002**, *21*, 4312−4314.

(18) de Bruin, B.; Peters, T. P. J.; Wilting, J. B. M.; Thewissen, S.; Smits, J. M. M.; Gal, A. W. *Eur. J. Inorg. Chem.* **2002**, *10*, 2671−2680.

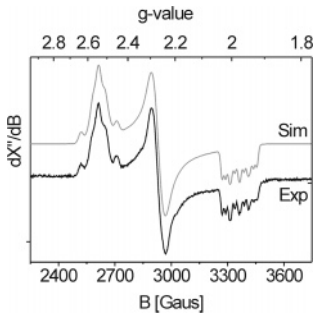

Figure 1. Experimental and simulated X-band EPR spectrum of $\mathbf{1}^{2+}$. Experimental conditions: Temperature = 10 K, microwave frequency = 9.30195 GHz, microwave power = 1 mW, field modulation amplitude = 2 G. The simulated spectrum was obtained with the parameters given in Table 1.

Table 1. Simulation (Exp.) and DFT−ADF Calculated EPR Parameters (10^{-4} cm^{-1}) from 1^{2+} (Figure 1)[a]

	g_1 (x)		g_2 (y)		g_3 (z)	
	exp	DFT	exp	DFT	exp	DFT
g-value	2.540	2.526	2.265	2.157	1.975	1.930
HFI_{Ir}	45	33	<20	25	46	53
$HFI_{N(amine)}$	<20	11	<20	11	17	18
NQI (η)	−10	−7	−16	−21	26 (0.23)	28 (0.51)

[a] η = NQI "rhombicity parameter".

room temperature; complete degradation requires more than 24 h, and results in a complex mixture of diamagnetic products. Decomposition of $\mathbf{2}^{2+}$ is accelerated upon passing N_2 gas through the solution (complete degradation within 30 min), and is therefore probably related to ethene loss.

EPR Spectroscopy. The X-band EPR spectrum of $\mathbf{1}^{2+}$ in frozen acetone/MeOH (40 K) is shown in Figure 1. Simulation of the rhombic spectrum yielded the following g-values: g_1 = 2.538, g_2 = 2.265 and g_3 = 1.975. The (super)hyperfine coupling pattern for the g_3 signal could be easily and satisfactorily simulated by assuming hyperfine coupling with iridium ($A_3^{Ir} = 46 \times 10^4$ cm^{-1}) and superhyperfine coupling with one nitrogen ($A_3^{N} = 17 \times 10^4$ cm^{-1}). Contributions from other N-nuclei are not resolved in this direction. The g_2 signal reveals no resolved hyperfine-coupling. In a previous communication we already discussed this EPR spectrum. At the time of writing, we did not understand the 5-line (super)hyperfine-coupling pattern of the g_1 signal. Deuteration experiments, DFT calculations and simulations have now revealed that a quadrupole distortion of the iridium hyperfine-coupling pattern is responsible for this strange signal. Details are given in the Supporting Information.

Although complex $\mathbf{1}^{2+}$ reacts with MeCN (see section 2.2), its lifetime in MeCN is sufficiently long for convenient EPR measurements in this solvent. The solvent is however of little influence. Apart from broadening due to a poorer glass, frozen solutions of $\mathbf{1}^{2+}$ in neat acetone (without MeOH), in neat MeCN (very broad spectrum), or in MeCN/0.1 M [(n-Bu)$_4$N](PF$_6$) (this salt is added to obtain a better glass) reveal comparable EPR spectra to the one shown in Figure 1. The EPR spectrum of $\mathbf{2}^{2+}$ is almost identical to that of $\mathbf{1}^{2+}$, with slightly different g-values and hyperfine interactions (Freq. = 9.299 GHz, acetone/MeOH (2:3), 40 K): g_1 = 2.52 (five-line pattern (1:4:6:4:1), $A^{Ir}_{11} \approx 47 \times 10^{-4}$ cm^{-1}), g_2 = 2.27 (no resolved hyperfine couplings), g_3 = 1.98 ($A_{33}^{Ir} = 43 \times 10^{-4}$ cm^{-1}, $A_{33}^{N} = 18 \times 10^{-4}$cm^{-1}).

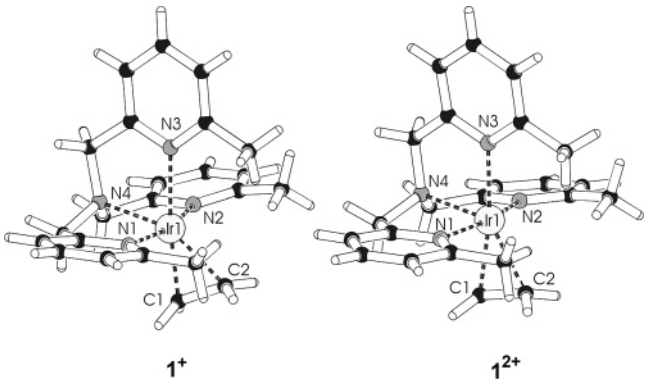

Figure 2. X-ray structures of Ir^{I}−ethene complex $\mathbf{1}^{+}$ (left) and Ir^{II}−ethene complex $\mathbf{1}^{2+}$ (right).

X-ray Diffraction. Crystals of $\mathbf{1}^{2+}$ suitable for X-ray diffraction were obtained from a dichloromethane solution of $\mathbf{1}^{2+}$ layered with hexane. The X-ray structures of $\mathbf{1}^{+}$ and $\mathbf{1}^{2+}$ are compared in Figure 2. The X-ray structure of $\mathbf{2}^{+}$ (not shown) was also determined. Selected bond lengths and angles of $\mathbf{1}^{+}$, $\mathbf{2}^{+}$, and $\mathbf{1}^{2+}$ are given in Table 2.

Complex $\mathbf{1}^{+}$ is best described as a distorted trigonal bipyramid with two pyridines of the Me$_3$tpa ligand at the apical positions and the third pyridine, the amine and the ethene moieties in the equatorial plane. The structure of $\mathbf{2}^{+}$ is similar to that of $\mathbf{1}^{+}$, except for the position of the ethene fragment. The decreased steric bulk of the Me$_2$tpa ligand allows the ethene fragment to be positioned closer to N3 (i.e., closer to an ideal tbp-equatorial position), as expressed by approximately 8° smaller C1−Ir1−N3 and C2−Ir1−N3 angles in $\mathbf{2}^{+}$ compared to $\mathbf{1}^{+}$ (Table 2).

Upon oxidation of $\mathbf{1}^{+}$ to $\mathbf{1}^{2+}$, the olefin moves to a position trans to the third pyridine group, i.e., the geometry of the complex changes to square pyramidal with the amine in the apical position and the pyridines and the ethene in the basal plane. Oxidation of $\mathbf{1}^{+}$ to $\mathbf{1}^{2+}$ results in a stronger binding of Me$_3$-tpa to Ir; the Ir−N3 distance shortens by ~0.12 Å, whereas the N1−Ir1, N2−Ir1, and N4−Ir1 distances do not change significantly (See Table 2). The shortening of the C1−C2 distance by 0.07 Å and the elongation of the Ir−C1 distance by 0.09 Å on going from $\mathbf{1}^{+}$ to $\mathbf{1}^{2+}$ indicates weakening of the Ir−ethene interaction upon oxidation of Ir^{I} to Ir^{II}. This is unlikely to result from decreased ethene → Ir σ-bonding, so the weaker interaction is apparently due to decreased Ir → ethene π-back-bonding.

Electrochemistry. For the redox couple $\mathbf{1}^{+}/\mathbf{1}^{2+}$ electrochemically reversible oxidation−reduction waves (ΔE = 68−70 mV, I_b/I_f = 1.0) were observed with cyclic voltammetry in CH$_2$Cl$_2$, acetone and MeCN. The redox couple $\mathbf{2}^{+}/\mathbf{2}^{2+}$ also gives rise to reversible waves in CH$_2$Cl$_2$ and acetone, but oxidation of $\mathbf{2}^{+}$ in MeCN is much less reversible (I_b/I_f = 0.4, 100 mV/s). The reactivity of the Ir^{II} complexes with coordinating solvents such as MeCN is described in section 2.2.

Less substituted analogues of $\mathbf{1}^{2+}$ and $\mathbf{2}^{2+}$ viz. [(Me$_1$tpa)Ir^{I}-(ethene)]$^{+}$ and [(tpa)Ir^{I}(ethene)]$^{+}$,[19,20] reveal entirely irreversible

(19) Krom, M.; Peters, T. P. J.; Coumans, R. G. E.; Sciarone, T. J. J.; Hoogboom, J. T. V.; ter Beek, S. I.; Schlebos, P. P. J.; Smits, J. M. M.; de Gelder, R.; Gal, A. W. *Eur. J. Inorg. Chem.* **2003**, *6*, 1072−1087.
(20) Kicken, R. J. N. A. M.; *Oxidation of Iridium Olefin Complexes by H_2O_2 and O_2*, Thesis 2001, University of Nijmegen.

Table 2. Selected Bond Lengths (Å) and Angles (deg) of **1**$^{+}$, **1**$^{2+}$, **2**$^{+}$, and **6**$^{2+}$

	1^{+} [(Me$_3$tpa)Ir(ethene)]$^{+}$	**1**$^{2+}$ [(Me$_3$tpa)Ir(ethene)]$^{2+}$	**2**$^{+}$ [(Me$_2$tpa)Ir(ethene)]$^{+}$	**6**$^{2+}$ [(Me$_3$tpa)Ir(NO)]$^{2+}$
Ir1−C1	2.042 (9)	2.136 (6)	2.073 (7)	
Ir1−C2	2.143 (9)	2.149 (6)	2.051 (7)	
Ir1−N1	2.075 (7)	2.071 (5)	2.039 (6)	2.062 (4)
Ir1−N2	2.043 (8)	2.062 (5)	2.066 (5)	2.058 (5)
Ir1−N3	2.260 (7)	2.136 (5)	2.219 (6)	2.193 (8)
Ir1−N4	2.154 (8)	2.146 (5)	2.153 (5)	2.126 (8)
Ir1−N5				1.753 (5)
C1−C2	1.451 (13)	1.380 (9)	1.442 (11)	
O5−N5				1.154 (9)
C1−Ir1−N3	173.3 (3)	172.0 (2)	164.5 (3)	
C2−Ir1−N3	132.8 (3)	150.2 (2)	124.7 (3)	
N5−Ir1−N3				144.6 (2)
Ir1−N5−O5				174.5 (7)

Table 3. Electrochemical Data for [(Me$_n$Tpa)Ir^{I}(ethene)]$^{+}$ (n = 0, 1, 2, 3)[a]

compd	solvent	E_p[b]	$E_{1/2}$[b]	ΔE[b]	I_b/I_f[b]
[(Me$_3$tpa)Ir^{I}(ethene)]$^{+}$ (**1**$^{+}$)	CH_2Cl_2	−255	−289	68	1.0
	acetone	−334	−368	70	1.0
	MeCN[c]	−330	−365	69	1.0
[(Me$_2$tpa)Ir^{I}(ethene)]$^{+}$ (**2**$^{+}$)	CH_2Cl_2	−138	−173	68	1.0
	acetone	−213	−249	70	1.0
	MeCN	−198	−240	84	0.4
[(Me$_1$tpa)Ir^{I}(ethene)]$^{+}$	CH_2Cl_2	−43			0
	Acetone	−122			0
	MeCN	−93			0
[(tpa)Ir^{I}(ethene)]$^{+}$	CH_2Cl_2	−136			0
	Acetone	−144			0
	MeCN	−10			0

[a] E in mV versus Fc/Fc^{+}. E_p: anodic peak potential, $E_{1/2}$: half-wave potential, ΔE: peak separation, I_b/I_f: cathodic peak current/anodic peak current. Scan rate 100 mV/s. [b] These data are for the 1+/2+ couple. [c] Complex **1** reveals an irreversible 2+/3+ couple in MeCN at E_p^a = 1100mV (initial current flow starts above 700 mV).

oxidation waves even in the weakly coordinating solvents CH_2Cl_2 and acetone (Table 3). In line with these observations, all attempts to prepare the corresponding iridium(II)-ethene species (less substituted analogues of **1**$^{2+}$ and **2**$^{2+}$) were unsuccessful.

Despite that, for steric reasons, 6-methylpyridyl donors are weaker donors than pyridine donors,[11d] 1e oxidation of Me$_3$tpa complex **1**$^{+}$ is more easy than 1e oxidation of Me$_2$tpa complex **2**$^{+}$. This is probably related to the fact that, with increasing n, the increasing steric bulk of the Me$_n$tpa ligands forces the geometry of the monocationic [(Me$_n$tpa)Ir^{I}(ethene)]$^{+}$ complexes to be closer to the preferred square pyramidal geometry of the dicationic Ir^{II} oxidized species (see Table 2). In line with this, 1e oxidation of [(Me$_1$tpa)Ir^{I}(ethene)]$^{+}$ and [(tpa)Ir^{I}(ethene)]$^{+}$ occurs at higher potentials than that of **2**$^{+}$. For the complexes with the least steric bulk, the increasing donor strength of the Me$_n$tpa ligands with decreasing n apparently counter-effects the above geometry effect, thus resulting in a more easy oxidation of [(tpa)Ir^{I}(ethene)]$^{+}$ relative to [(Me$_1$tpa)Ir^{I}(ethene)]$^{+}$.

2.2 Reactivity of Ir^{II}(ethene) toward Closed-Shell Ligands. It was earlier reported by Wayland and co-workers, that [(por)-Rh^{II}] complexes (por^{2-} = a bulky meso-tetra-arylporphyrinate dianion) have a higher affinity for CO than for ethene.[21] Neither **1**$^{2+}$ nor **2**$^{2+}$ shows any reaction with CO (except for ethene loss from **2**$^{2+}$ also observed with N_2). The difference in CO affinity between the [(por)Rh^{II}] systems and **1**$^{2+}$/**2**$^{2+}$ may arise from the stronger σ-donor character of the anionic por^{2-} ligands compared to our neutral Me$_n$tpa ligands.

According to Wayland, ethene complexes [(por)M^{II}(ethene)] (M = Rh, Ir; generated in situ from [(por)M^{II}] and ethene) are not stable. Dependent on the ligand bulk, they undergo bimolecular M−C coupling to ethylene bridged species [(por)-M^{III}−CH$_2$CH$_2$−M^{III}(por)] or bimolecular C−C coupling to form butylene bridged species [(por)M−CH$_2$CH$_2$−CH$_2$CH$_2$−M-(por)]. Apparently, in [(por)M^{II}(ethene)] the unpaired electron has a relatively high density on the ethene substrate, imposing some M^{III}-ethyl radical character on these transient species.[8g,14,15a]

Scheme 3. Formation of Ethylene Bridged Dinuclear Species from [(Me$_n$Tpa)Ir^{II}(ethene)]$^{2+}$ (n = 2, 3) in Acetonitrile

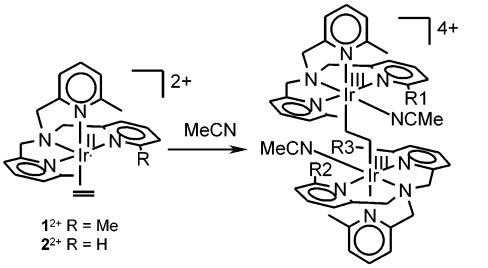

Our complexes **1**$^{2+}$ and **2**$^{2+}$ do not spontaneously couple to butylene-bridged species in weakly coordinating solvents such as acetone. Upon dissolving **1**$^{2+}$ in the coordinating solvent acetonitrile however, the complex slowly and selectively converts to ethylene-bridged species **3**$^{4+}$. Full conversion of **1**$^{2+}$ to **3**$^{4+}$ requires approximately 2−3 h. The sterically less hindered complex **2**$^{2+}$ is more reactive and in MeCN instantaneously and selectively converts to a 1:1 mixture of diastereomers **4a**$^{4+}$ and **4b**$^{4+}$ (Scheme 3). The increased reactivity with MeCN of **2**$^{2+}$ over the more hindered analogue **1**$^{2+}$ is indicative for an associative step in the reaction mechanism, either as the rate-limiting step or in a (concentration limiting) pre-equilibrium.

Figure 3 shows the structure of **4b**$^{4+}$; selected bond lengths and angles for **3**$^{4+}$ and **4b**$^{4+}$ are given in Table 4.

According to ^{1}H NMR, other nitrile donors such as benzonitrile also induce formation of ethylene-bridged species similar to **3**$^{4+}$ and **4**$^{4+}$. Donor-induced coupling is also observed with chloride as a donor, but this reaction is very nonselective.[22] Treatment of **2**$^{2+}$ with chloride yields about 5% (by ^{1}H NMR) of **5**$^{2+}$, which is similar to **4**$^{4+}$ but contains chloro ligands instead of MeCN. From the 1:1 mixture of diastereomers **5a**$^{2+}$ and **5b**$^{2+}$,

(21) Basickes, L.; Bunn, A. G.; Wayland, B. B. *Can. J. Chem.* **2001**, *79*, 854−856.

(22) The observed aselectivity of the reaction with Cl^{-} is presently not understood. This could be somehow related to Cl^{-} induced disproportionation of Rh^{II}(nbd) (nbd = 1,5-norbornadiene) complexes upon addition of Cl^{-}: see ref 11d.

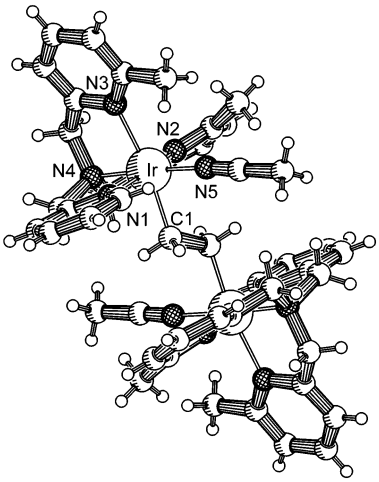

Figure 3. X-ray structure of $\mathbf{4b}^{4+}$.

Table 4. Selected Bond Lengths (Å) and Angles (deg) of $\mathbf{3}^{4+}$, $\mathbf{4b}^{4+}$, and $\mathbf{5b}^{2+}$

	$\mathbf{3}^{4+}$	$\mathbf{4b}^{4+}$	$\mathbf{5b}^{2+}$
Ir1−N1	2.093 (4)	2.041 (5)	2.087 (3)
Ir1−N2	2.103 (5)	2.073 (5)	2.040 (3)
Ir1−N3	2.270 (4)	2.257 (5)	2.281 (3)
Ir1−N4	2.041 (4)	2.034 (5)	2.043 (3)
Ir1−N5	2.007 (4)	2.020 (5)	
Ir1−Cl1			2.3787 (11)
Ir1−C1	2.105 (5)	2.116 (5)	2.102 (4)
C1−C1′	1.501 (7)	1.510 (11)	1.518 (8)
Ir1−C1−C1′	117.7 (4)	118.0 (5)	117.7 (4)

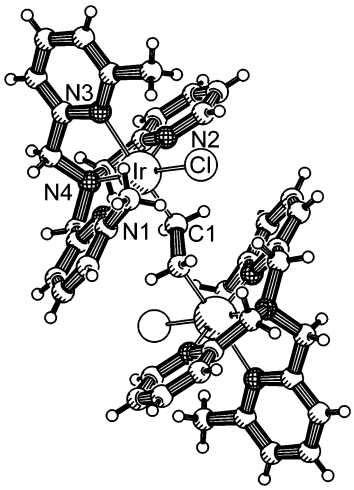

Figure 4. X-ray structure of $\mathbf{5b}^{2+}$.

$\mathbf{5b}^{2+}$ selectively crystallized; the structure is shown in Figure 4, selected bond lengths and angles are given in Table 4.

Complexes $\mathbf{3}^{4+}$, $\mathbf{4b}^{4+}$, and $\mathbf{5b}^{2+}$ are the first examples of structurally characterized products of Ir• and •CH_2CH_2Ir coupling, and thus provide support for the formulation as ethylene-bridged species of the (por)Ir−CH_2CH_2−Ir(por) complexes mentioned above, none of which were characterized by X-ray diffraction.

2.3 Reactivity of Ir^{II}(ethene) toward Radicals. 2.3.1 Reactions with NO. When a solution of $\mathbf{1}(PF_6)_2$ in acetone was subjected to an atmosphere of gaseous NO at −78 °C a color change from greenish black to brown was observed within 15 min. According to ^{1}H NMR, the reaction is associated with release of ethene and selectively yields a single diamagnetic (Me_3tpa)Ir product (Scheme 4).

Scheme 4. Reaction of $\mathbf{1}^{2+}$ with Nitrogen Monoxide

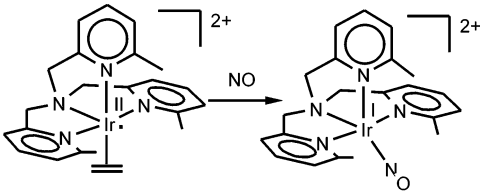

$\mathbf{1}^{2+}$ $\mathbf{6}^{2+}$

The resulting complex $\mathbf{6}^{2+}$ shows a strong absorption at $\nu = 1800$ cm^{-1} in the IR spectrum, typical for a terminal, linear nitrosyl group.[23] Complex $\mathbf{6}^{2+}(PF_6)_2$ could also be obtained by treatment of iridium(I) compound $\mathbf{1}^+(PF_6)$ with $NO^+(PF_6)$ in acetone. Since NO^+ is a very strong oxidant (its reduction potential lies approximately 600 mV above that of Fc^+), this could well proceed via initial oxidation of $\mathbf{1}^+$ to $\mathbf{1}^{2+}$ by NO^+, followed by radical coupling of $\mathbf{1}^{2+}$ with thus generated NO as above. Both reactions are associated with formation of 4-hydroxy-4-methylpentan-2-one ('diacetone-alcohol'), and it seems that $\mathbf{6}^{2+}$ or one of its precursors slowly catalyzes the aldol condensation of acetone. Remarkably, reactions of $\mathbf{1}^+$ with NO^+ or $\mathbf{1}^{2+}$ with NO are unselective in MeCN.

To our knowledge, the reaction in Scheme 4 is the first well-documented example of radical capture by Ir^{II}. Radical capture of NO by (por^{2-})Rh^{II} metallo-radicals, similar to the reaction in Scheme 4, has been reported previously.[24] Apart from its unusual synthesis, nitrosyl complexes of iridium similar to of $\mathbf{6}^{2+}$ are not unprecedented. Many Ir−NO complexes with monodentate, inorganic ligands have been prepared, but complexes with organic polydentate ligands are less abundant.[25,26] Examples of linear, bent and bridged complexes have been reported, and among these are also iridium−NO−olefin complexes (cyclooctadiene and even ethene).[26] This is in contrast with the observed ethene loss upon formation of $\mathbf{6}^{2+}$.

The crystal structure of $\mathbf{6}^{2+}$ (Figure 5, selected bond lengths and angles are given in Table 2) confirms the presence of a linear nitrosyl group. The linear NO fragment can be regarded as an NO^+ fragment coordinated to an iridium center in the formal oxidation state +I. Indeed, the structure of $\mathbf{6}^{2+}$ is fairly similar to that of $\mathbf{1}^+$, with cationic NO^+ replacing neutral C_2H_4. The Ir−N2 distance is slightly longer in $\mathbf{6}^{2+}$ compared to $\mathbf{1}^{2+}$, in contrast to the Ir−N1, Ir−N3, and Ir−N4 distances, which are slightly shorter. The observed Ir−N5 (1.754 Å) and N−O (1.155 Å) lengths are typical for this type of compounds.[27]

So, the radical coupling of two molecules $\mathbf{1}^{2+}$ or $\mathbf{2}^{2+}$ to give the Ir^{III}−CH_2−CH_2−Ir^{III} binuclear complexes $\mathbf{3}^{4+}$, $\mathbf{4}^{4+}$, or $\mathbf{5}^{2+}$ (see Section 2.2) indicates at least some radical character of the ethene ligand, but the reaction of $\mathbf{1}^{2+}$ with NO in acetone

(23) Ford, P. C.; Lorkovic, I. M. *Chem. Rev.* **2002**, *102*, 993.
(24) Wayland, B. B.; Newman, A. R. *Inorg. Chem.* **1981**, *20*, 2093.
(25) Heyton, T. W.; Legzdins, P.; Sharp, W. B. *Chem. Rev.* **2002**, *102*, 935.
(26) See for example (a) Batchelor, R. J.; Einstein, F. W. B.; Lowe, N. D.; Palm, B. A.; Yan, X.; Sutton, D. *Organometallics* **1994**, *13*, 2041. (b) Jenkins, H. A.; Loeb, S. J. *Organometallics* **1994**, *13*, 1840. (c) Matsukawa, S.; Kuwata, S.; Hidai, M. *Inorg. Chem.* **2000**, *39*, 791.
(27) (a) Matsukawa, S.; Kuwata, S.; Hidai, M. *Inorg. Chem.* **2000**, 39, 791. (b) Cheng, P. T.; Nyburg, S. C. *Inorg. Chem.* **1975**, *14*, 327. (c) Clark, G. R.; Waters, J. M.; Whittle, K. R. *Inorg. Chem.* **1974**, *13*, 1628. (d) Pratt, C. S.; Ibers, J. A. *Inorg. Chem.* **1972**, *11*, 2812. (e) Batchelor, R. J.; Einstein, F. W. B.; Lowe, N. D.; Palm, B. A.; Yan, X.; Sutten, D. *Organometallics* **1994**, *13*, 2041. (f) Boyar, E. B.; Moore, D. S.; Robinson, S. D.; James, B. R.; Preece, M.; Thorburn, T. *J. Chem. Soc., Dalton Trans.* **1985**, 617.

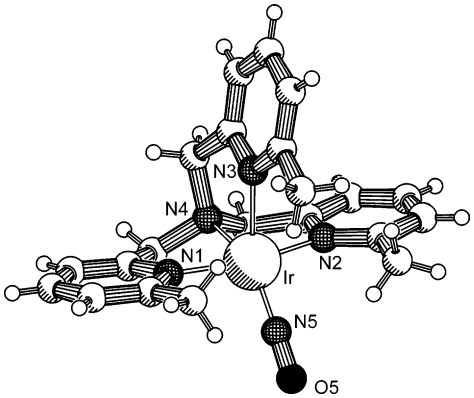

Figure 5. X-ray structure of $\mathbf{6}^{2+}$.

Scheme 5. Formation of $\mathbf{7}^{2+}$ from $\mathbf{1}^{2+}$ and TEMPO and Subsequent Hydrolysis of $\mathbf{7}^{2+}$ to $\mathbf{8}^{2+}$

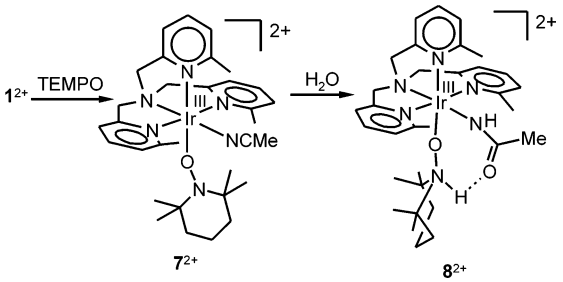

to give Ir−NO complex $\mathbf{6}^{2+}$ indicates metallo-radical character. Apparently Ir^{II}(ethene) allows reactions at both the metal and at the ethene fragment.[28]

2.3.2 Reactions with TEMPO. Addition of $\mathbf{1}(PF_6)_2$ to a solution of the nitroxyl radical TEMPO (2,2,6,6-tetramethyl-1-piperidinyloxo) in CH_3CN resulted in a dark brown solution. This solution turned yellow within 2 h, and ^1H NMR indicated formation of a diamagnetic product. Judging from the peaks in the spectra, ethene was expelled during the reaction, and a reduced TEMPO moiety as well as one molecule of acetonitrile was coordinated to the iridium, now present in oxidation state +III.

Interestingly, the initial product ($\mathbf{7}^{2+}$) selectively converted to a follow-up product ($\mathbf{8}^{2+}$) on standing in an acetonitrile solution for several days (Scheme 5).

If a few drops of water were added to a solution of $\mathbf{7}^{2+}$, conversion to $\mathbf{8}^{2+}$ required only 2 h. Complex $\mathbf{8}^{2+}$ contains an N-bound acetamido fragment and the reduced TEMPO is now N-protonated to give a κ^1-*O*−TEMPO*H* fragment. Complex $\mathbf{8}^{2+}$ must have formed by attack of H_2O to the nitrile triple bond of the coordinated MeCN fragment of $\mathbf{7}^{2+}$. The structure of $\mathbf{8}^{2+}$ was confirmed by X-ray diffraction (Figure 6, Table 5).

The geometry of $\mathbf{8}^{2+}$ is best described as distorted octahedral. The TEMPO*H* oxygen atom (O2) is positioned cis to the tpa amine nitrogen (N4). As expected for an N-bound acetamido fragment, the C1−O1 distance (1.263(2) Å) is significantly shorter than the C1−N5 distance (1.310(7) Å). The acetamido fragment is positioned trans to the tpa amine (N4).

The long N(6)−O(2) bond (1.423 Å) and the pyramidal geometry of N(6) [C(3)−N(6)−O(2) 109.5°, C(7)−N(6)−O(2) 109.4°] indeed indicate that the κ^1-*O*−TEMPO*H* ligand is fully reduced.[29] Therefore, this fragment should be regarded as an N-protonated TEMPO anion coordinated to Ir^{III} rather than an organic radical antiferromagnetically coupled to an Ir^{II} metallo-radical.

(28) Possibly, the observed nonselective reaction in MeCN is related to ligand radical behavior in this solvent.

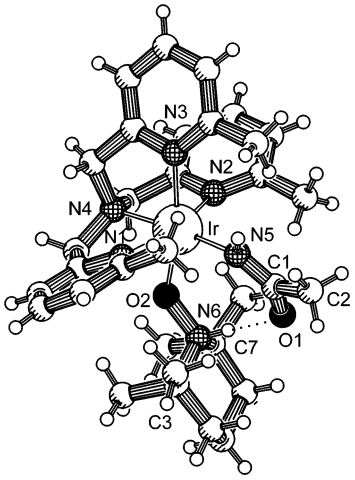

Figure 6. X-ray structure of $\mathbf{8}^{2+}$.

Table 5. Selected Bond Lengths (Å) and Angles (deg) of $\mathbf{8}^{2+}$

	$\mathbf{8}^{2+}$
Ir1−N1	2.113 (5)
Ir1−N2	2.101 (3)
Ir1−N3	2.131 (9)
Ir1−N4	2.055 (9)
Ir1−N5	2.073 (5)
Ir1−O2	1.423 (6)
C1−N5	1.310 (7)
C1−C2	1.514 (2)
C1−O1	1.263 (2)
N6....O1	2.646
O1....O2	3.333
Ir1−N5−C1	138.25 (16)
Ir1−O2−N6	129.10 (11)
C2−C1−N5	117.7 (7)
C2−C1−O1	117.9 (0)
N5−C1−O1	124.3 (2)
C3−N6−C7	116.7 (2)
C3−N6−O2	109.5 (9)
C7−N6−O2	109.4 (1)

We are aware of only one other crystallographically characterized transition metal complex with a η^1-O-bound TEMPO*H* fragment, i.e., [(F_6-acac)$_2$(formato)Fe(μ_2-O)Fe(F_6-acac)$_2$(TEMPO*H*)] (TEMPO*H* = N-protonated reduced TEMPO, F_6–acac = 1,1,1,5,5,5-hexafluoropentane-2,4-dionato-*O*,*O*′).[30] Transition metal complexes with reduced TEMPO ligands are rare,[31,32] especially those which exhibit a η^1-O-coordination,

(29) Mahanthappa, M. K.; Huang, K.-W.; Cole, A. P.; Waymouth, R. M.; *Chem. Commun.* **2002**, 502.
(30) Ahlers, C.; Dickman, M. H. *Inorg. Chem.* **1998**, *37*, 6337.
(31) Most transition metal TEMPO complexes contain neutral TEMPO radical ligands: (a) Dickman, M. H.; Doedens, R. J. *Inorg. Chem.* **1981**, *20*, 2677. (b) Porter, L. C.; Dickman, M. H.; Doedens, R. J. *Inorg. Chem.* **1983**, *22*, 1962. (c) Porter, L. C.; Dickman, M. H.; Doedens, R. J. *Inorg. Chem.* **1986**, *25*, 678. (d) Dong, T.-Y.; Hendrickson, D. N.; Felthouse, T. R.; Shieh, H.-S. *J. Am. Chem. Soc.* **1984**, *106*, 5373. (e) Felthouse, T. R.; Dong, T.-Y.; Hendrickson, D. N.; Shieh, H.-S.; Thompson, M. R. *J. Am. Chem. Soc.* **1986**, *108*, 8201. (f) Dickman, M. H.; Porter, L. C.; Doedens, R. J. *Inorg. Chem.* **1986**, *25*, 2595. (g) Anderson, O. P.; Keuchler, T. C. *Inorg. Chem.* **1980**, *19*, 1417. (h) Griesar, K.; Haase, W.; Svoboda, I.; Fuess, H. *Inorg. Chim. Acta* **1999**, *287*, 181. (i) Laugier, J.; Latour, J.-M.; Caneschi, A.; Rey, P. *Inorg. Chem.* **1991**, *30*, 4474. (j) Cogne, A.; Beolorizky, E.; Laugier, J. L.; Rey, P. *Inorg. Chem.* **1994**, *33*, 3364. (k) Seyler, J. W.; Fanwick, P. E.; Leidner, C. R. *Inorg. Chem.* **1992**, *31*, 3699. (l) Baskett, M.; Lathi, P. M.; Palacio, F. *Polyhedron* **2003**, *22*, 2363.

Scheme 6. Relative Energies of $\mathbf{1}^{2+}$, $\mathbf{9}^{2+}$, and $\mathbf{10}^{2+}$ (kcal/mol) as Obtained by DFT (b3-lyp) Calculations

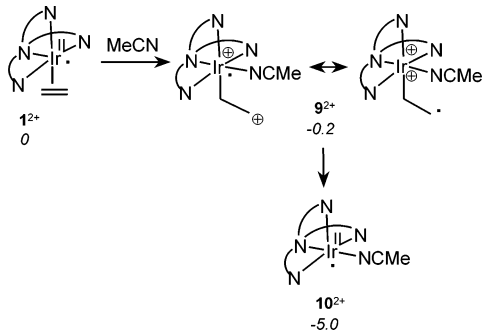

which has so far only been observed for titanium and iron.[29,30,33] Complexes $\mathbf{7}^{2+}$ and $\mathbf{8}^{2+}$ are the first examples of late transition metal complexes with a η^1-O-bound reduced TEMPO moiety. For $[Ti^{IV}(Cp)_2(Cl)(TEMPO)]$, homolytic splitting of the $Ti^{IV}-O^{TEMPO}$ bond at 60 °C results in formation of Ti^{III} and TEMPO radicals.[33b] Heating our complexes $\mathbf{7}^{2+}$ and $\mathbf{8}^{2+}$ to 50−80 °C resulted in unselective reactions.

In acetone, the reaction of $\mathbf{1}^{2+}$ with TEMPO is very slow and only gives unidentified mixtures, whereas in acetonitrile the formation of $\mathbf{7}^{2+}$ is much cleaner and faster. The approximate rate of formation of $\mathbf{7}^{2+}$ is comparable to that of $\mathbf{3}^{4+}$ in the absence of TEMPO. Yet, in the presence of TEMPO, selective formation of $\mathbf{7}^{2+}$ without $\mathbf{3}^{4+}$ is observed. This suggests that $\mathbf{7}^{2+}$ and $\mathbf{3}^{4+}$ result from the same precursor. Subsequent reaction of this intermediate with TEMPO must be much faster than its coupling to the $Ir^{III}-CH_2-CH_2-Ir^{III}$ dinuclear complex $\mathbf{3}^{2+}$.

2.4 DFT Geometry and Electronic Structure of Ir^{II}-(ethene), Ir^{II}(ethene)(NCMe) and Ir^{II}(NCMe). The different reactivity patterns observed for $\mathbf{1}^{2+}$ and $\mathbf{2}^{2+}$ in acetonitrile compared to acetone clearly show that the solvent plays an important role in the chemistry of these species. One might argue that changing the polarity of the solvent could influence the distribution of the spin density over the metal and the olefin fragment, without direct solvent coordination. In other words, the relative contribution of the two resonance structures in Scheme 1 to the electronic structure of $\mathbf{1}^{2+}$ could vary from solvent to solvent. However, frozen solutions of $\mathbf{1}^{2+}$ in acetone and acetonitrile reveal very comparable EPR spectra (see section 2.1), thus indicating that the influence of the solvent on the electronic structure of $\mathbf{1}^{2+}$ is small. So solvent coordination to the metal is more likely to play a role. To rationalize this difference in reactivity, we will consider three different metallo-radical species; that is Ir^{II}(ethene) complex $\mathbf{1}^{2+}$, its MeCN adduct $\mathbf{9}^{2+}$ and complex $\mathbf{10}^{2+}$ in which MeCN has been substituted for ethene (Scheme 6). To gain some understanding of their geometrical and electronic structure, we optimized the geometry of these species with DFT (b3-lyp).

(32) Anionic TEMPO ligands are usually η^2-*N, O* coordinated: (a) Jaitner, P.; Huber, W.; Huttner, G.; Scheidsteger, O. *J. Organomet. Chem.* **1983**, *259*, C1−C5. (b) Jaitner, P.; Huber, W.; Gieren, A.; Betz, H. *J. Organomet. Chem.* **1986**, *311*, 379−385. (c) Jaitner, P.; Huber, W.; Gieren, A.; Betz, H. *Z. Anorg. Allg. Chem.* **1986**, *538*, 53−60. (d) Dickman, M. H.; Doedens, R. J. *Inorg. Chem.* **1982**, *21*, 682−684. (e) Okunaka, M.; Matsubayashi, G.; Tanaka, T. *Bull. Chem. Soc. Jpn.* **1977**, *50*, 1070−1073. (f) Jaitner, P.; Huber, W. *Inorg. Chim. Acta* **1987**, *129*, L45−L46. (g) Mindiola, D. J.; Waterman, R.; Jenkins, D. M.; Hillhouse, G. L. *Inorg. Chim. Acta* **2003**, *345*, 299−308.

(33) (a) Evans, W. J.; Perotti, J. M.; Doedens, R. J.; Ziller, J. W. *Chem. Commun.* **2001**, 2326−2327. (b) Huang, K.-W.; Waymouth, R. M. *J. Am. Chem. Soc.* **2002**, *124*, 8200.

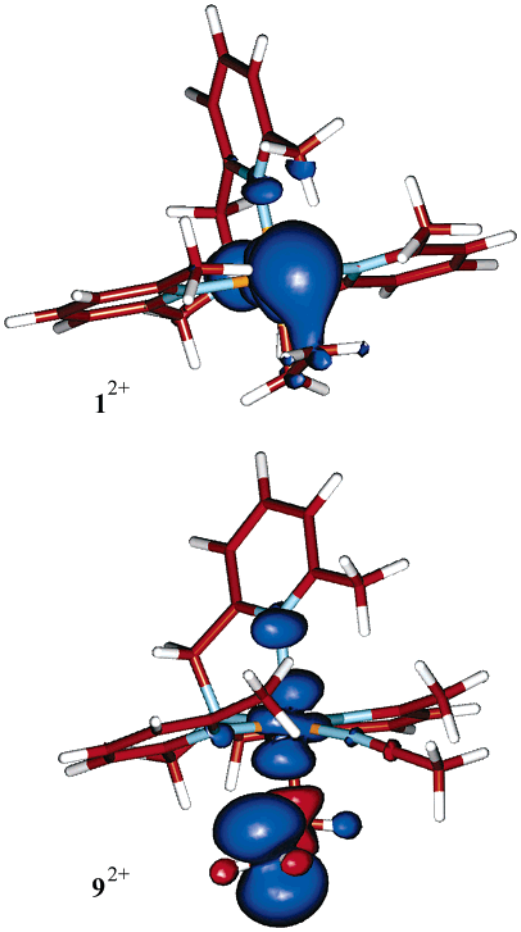

Figure 7. Spin density plots of the DFT optimized structures of $\mathbf{1}^{2+}$ (top) and $\mathbf{9}^{2+}$ (bottom).

The complexes $\mathbf{1}^{2+}$, $\mathbf{9}^{2+}$, and $\mathbf{10}^{2+}$ lie very close in energy (Scheme 6). These values are not corrected for ZPE and thermal contributions; the *free* energy of $\mathbf{9}^{2+}$ must be somewhat higher and that of $\mathbf{10}^{2+}$ lower than presented.[34]

Complex $\mathbf{10}^{2+}$ bears only hard, innocent N-donor ligands and must therefore represent a metallo-radical, with its unpaired electron almost entirely located at the iridium center. For the complexes $\mathbf{1}^{2+}$ and $\mathbf{9}^{2+}$ the electronic structure is less obvious. Ethene is a potentially "non-innocent" ligand, in the sense that in open-shell systems an unpaired electron could well be located at the coordinated ethene fragment instead of the metal center.

The observed large *g*-anisotropy observed in the EPR spectrum of complex $\mathbf{1}^{2+}$ can only arise from large orbital contributions induced by strong spin−orbit couplings from the heavy iridium atom. From this, we must conclude that the unpaired electron of $\mathbf{1}^{2+}$ mainly resides at the iridium-center. Indeed, a spin-density plot of the DFT optimized (b3-lyp) geometry of $\mathbf{1}^{2+}$ (Figure 7) reveals a mainly iridium centered distribution of spin density with only minor delocalization to the coordinated ethene fragment. Upon coordination of MeCN to $\mathbf{1}^{2+}$ however, the spin density shifts significantly from the metal to the ethene fragment.

The DFT geometry of $\mathbf{9}^{2+}$ is remarkable. The ethene fragment coordinates in a "slipped" way, leading to an iridium-alkyl type

(34) The entropy contribution for an incoming MeCN fragment in acetonitrile solution should be quite low, but this is not easily calculated with the applied gas-phase type calculations.

interaction. The octahedral geometry around iridium is severely distorted, with a very long Ir−N distance (2.41 Å) of the pyridyl fragment trans to Ir−C_{ethene}. This is most likely the result of the strong trans-influence of the unusual (alkyl type) slipped ethene fragment and/or additional repulsion imposed by the unpaired electron density in this direction (resulting in a bond order <1 for binding between Ir and this N-donor). Whereas the α-carbon of the slipped olefin fragment seems to be tetrahedral and sp^3 hybridized, the β-carbon atom is planar and sp^2-hydridized. Both the slipped-olefin description $Ir^{II}-CH_2-CH_2^{\oplus}$ and the ethyl radical description $Ir^{III}-CH_2-CH_2^{\bullet}$ would fit to this geometry. The spin-density plot (Figure 7) reveals that neither of these descriptions is completely appropriate and the actual electronic structure is intermediate between the two resonance structures depicted in Scheme 6, in which the $Ir^{III}-CH_2-CH_2^{\bullet}$ description prevails. Unfortunately, we were not able to directly detect $\mathbf{9}^{2+}$ with EPR. So, we cannot provide any supporting experimental data. Nevertheless, it seems reasonable to assume $\mathbf{9}^{2+}$ and $\mathbf{10}^{2+}$ as intermediates in the chemistry of $\mathbf{1}^{2+}$ in MeCN, based on the calculated relative energies.

2.5 Discussion. 2.5.1 Reactivity of (metallo) Radicals. Coordinating solvents, in particular acetonitrile, seem to play an important role in the observed reactions. The coupling of two Ir^{II}(ethene) species to dinuclear $Ir-CH_2-CH_2-Ir$ species (section 2.2) and the reaction of Ir^{II}(ethene) with TEMPO (section 2.3.2) lead to MeCN adducts. In other solvents these reactions do not proceed and/or lead to (slow) decomposition to give mixtures. We will now try to rationalize our observations assuming the involvement of the solvent adducts $\mathbf{9}^{2+}$ and $\mathbf{10}^{2+}$ (Scheme 6) as intermediates.

As described in section 2.2, donor solvents and other coordinating reagents such as MeCN, PhCN and Cl^- apparently trigger ethene dissociation and M−C coupling of Ir^{II} and Ir^{II}-(ethene). We studied the reactions of complexes $\mathbf{1}^{2+}$ and $\mathbf{2}^{2+}$ with MeCN in detail; the related products obtained from reaction of $\mathbf{1}^{2+}$ with Cl^- and PhCN probably proceed in a similar way. The reaction rate increases strongly on going from Me_3tpa complex $\mathbf{1}^{2+}$ to the more accessible Me_2tpa complex $\mathbf{2}^{2+}$. The methyl groups of the three 6-methylpyridyl donors of $\mathbf{1}^{2+}$ are primarily directed to the vacant site cis to the olefin fragment (the exact spot where MeCN should coordinate) and seem to have little steric influence on the approach of two complexes to form the ethylene bridge. This suggests the importance of solvent coordination prior to the actual M−C coupling. In view of the radical type mechanisms proposed for formation of the species $[(por)M^{III-}CH_2CH_2-M^{III}(por)]$ and $[(por)M^{III}-CH_2-CH_2-CH_2CH_2-M^{III}(por)]$ from $[(por)M^{II}]$ and ethene (M = Rh, Ir),[8g,14,15a] it is tempting to propose a similar radical pathway for formation of $\mathbf{3}^{4+}$ and $\mathbf{4a}^{4+}/\mathbf{4b}^{4+}$ (Scheme 7). Most likely, acetonitrile coordinates to $\mathbf{1}^{2+}$ to give $\mathbf{9}^{2+}$. Subsequent elimination of ethylene then results in formation of $\mathbf{10}^{2+}$.[35] It seems reasonable to propose that the selective formation of $\mathbf{3}^{4+}$ proceeds via associative substitution of MeCN for ethene to give the reactive metallo-radical $\mathbf{10}^{2+}$, followed by a radical coupling (with unreacted $\mathbf{1}^{2+}$ or with $\mathbf{9}^{2+}$). Alternatively, one could envisage coordination of MeCN to trigger disproportionation to Ir^I and Ir^{III} species, which could then couple via electrophilic attack of Ir^{III} at Ir^I(ethene).[22] Disproportionation of $\mathbf{1}^{2+}$ to $\mathbf{1}^{+}$ and $\mathbf{1}^{3+}$ in MeCN is however endothermic by at least $\Delta G^0 \geq 24$ kcal/mol, as determined from the cyclic voltammetry data for $\mathbf{1}^{2+}$ and $\mathbf{2}^{2+}$, which seems to be too high to be compatible with the instantaneous conversion of $\mathbf{2}^{2+}$ to $\mathbf{4a}^{4+}/\mathbf{4b}^{4+}$ in MeCN.

Scheme 7. Proposed Mechanism for the Formation of $\mathbf{3}^{4+}$ and $\mathbf{7}^{2+}$

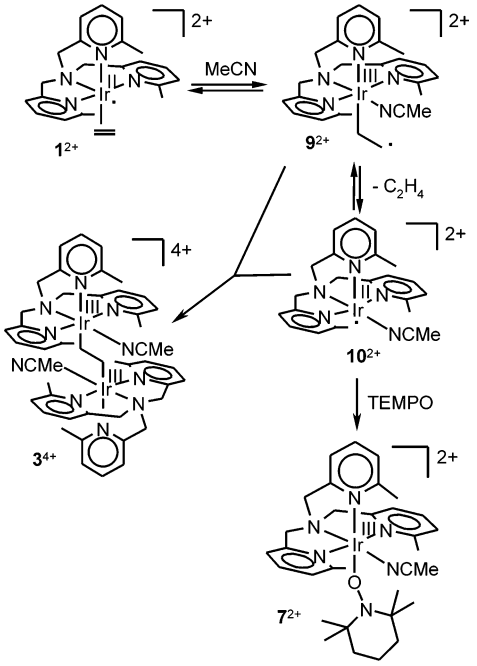

Full conversion of $\mathbf{1}^{2+}$ to $\mathbf{7}^{2+}$ in the presence of TEMPO or to $\mathbf{3}^{4+}$ in the absence of TEMPO takes roughly similar reaction times. A reasonable explanation would be that $\mathbf{7}^{2+}$ and $\mathbf{3}^{4+}$ are formed via a common intermediate (presumably $\mathbf{10}^{2+}$) attacking either TEMPO or $\mathbf{1}^{2+}/\mathbf{9}^{2+}$. The preferential formation of the TEMPO adduct could be due to a lower radical character of the olefinic carbon of $\mathbf{1}^{2+}$ and/or lower concentration of $\mathbf{9}^{2+}$, compared to TEMPO.

In weakly coordinating solvents such as acetone, TEMPO does not react cleanly with $\mathbf{1}^{2+}$ and $\mathbf{2}^{2+}$. Apparently, direct attack is prevented by steric hindrance, and formation of a more open radical like $\mathbf{10}^{2+}$ is required. In contrast, the small radical NO directly combines with $\mathbf{1}^{2+}$. Radical coupling of TEMPO with complex $\mathbf{9}^{2+}$ (at carbon) might also be expected, but was not observed. This suggests that $\mathbf{9}^{2+}$ is only present in very low concentrations and/or $\mathbf{10}^{2+}$ is much more reactive. The choice of TEMPO attack to the metal instead of the olefin may be kinetically determined.

2.5.2 Attack of Water at Coordinated MeCN. Although activation of nitriles by coordination to a transition metals seems straightforward,[36,37] there may be a kinetic problem for attack of H_2O to a linearly coordinated nitrile fragment. For example, the iridium complex $[(Cp^*)(\eta^3\text{-}CH_2CHCHPh)Ir^{III}(NCMe)]^+$ (to stay close to the compounds in this paper), is a catalyst for the hydrolysis of nitriles. However, attack of water to the coordi-

(35) Upon spraying a sample of $\mathbf{1}^{2+}$ in MeCN, masses corresponding to $\mathbf{14}^{2+}$ and $\mathbf{15}^{2+}$ were detected with ESI−MS. This observation can however not be regarded as direct evidence for the mechanism proceeding via $\mathbf{14}^{2+}$ and $\mathbf{15}^{2+}$, because these species may stem from fragmentation of already formed $\mathbf{3}^{4+}$. Spraying an isolated pure sample of $\mathbf{3}^{4+}$ reveals these same masses.

(36) Michelin, R. A.; Mozzon, M.; Bertani, R. *Coordin. Chem. Rev.* **1996**, 147, 299.

(37) Chin, C. S.; Chong, D.; Lee, B.; Jeong, H.; Won, G.; Do, Y.; Park, Y. J. *organometallics*, **2000**, *19*, 638, and references therein.

nated nitrile of the isolated complex to give a (deprotonated) amide requires elevated temperatures (reflux for 3 h in a MeCN/H_2O/Na_2CO_3 mixture) and the reaction becomes catalytic only at 70 °C in the presence of Na_2CO_3. Also, if we compare the MeCN adducts in this paper we see large differences in the affinity of coordinated nitriles for water. The MeCN fragment of dinuclear compound $\mathbf{3}^{4+}$—which resembles $\mathbf{7}^{2+}$ in the coordinated MeCN ligand and in the formal charge of the metal center—is not hydrolyzed in the mere presence of water at room temperature. This difference is even more remarkable considering that the steric hindrance around the nitrile in $\mathbf{3}^{4+}$ is far less than in $\mathbf{7}^{2+}$. Thus, the TEMPO anion in $\mathbf{7}^{2+}$ must be assisting in the attack of water through its ability to form hydrogen bridges.

Conclusions

In weakly coordinating solvents, the 17 VE $[(N_4\text{-ligand})Ir^{II}(\text{ethene})]^{2+}$ species seem to reflect metallo-radical behavior, as illustrated by the capture of NO. In strongly coordinating solvents such as MeCN, they seem to react via initial formation of MeCN adducts $[(N_4\text{-ligand})Ir(\text{ethene})(MeCN)]^{2+}$. DFT calculations suggest that the electronic structure of these species is somewhere between a 19 VE metallo-radical Ir^{II}(ethene) species and a 18 VE Ir^{III}-ethyl radical species. The MeCN adducts easily lose ethene to form 17 VE $[(N_4\text{-ligand})Ir^{II}(MeCN)]^{2+}$ metallo-radicals, which are less hindered and efficiently capture other radicals such as TEMPO or $Ir^{III}-CH_2-CH_2\cdot/Ir^{II}$(ethene). Finally, the donor-induced shifting of spin density from metal to olefin constitutes a new approach to tuning the reactivity of open-shell metal-olefin complexes.

Experimental Section

General Procedures. All procedures were performed under N_2 with standard Schlenk techniques unless indicated otherwise. Acetonitrile was purified and deoxygenated by distillation over CaH_2 under N_2. All other solvents (p.a) were deoxygenated by bubbling through a stream of N_2 or by freeze−pump−thaw method. The temperature indication room temperature (RT) corresponds to about 20 °C. NMR experiments were carried out on a Bruker DPX200 (200 and 50 MHz for ^{1}H and ^{13}C, respectively) and a Bruker AC300 (300 and 75 MHz for ^{1}H and ^{13}C, respectively). Solvent shift reference for ^{1}H spectroscopy: [D$_6$]-acetone $\delta_H = 2.05$, [D$_3$]-acetonitrile $\delta_H = 1.94$. For ^{13}C NMR: [D$_6$]-acetone $\delta_C = 29.50$, [D$_3$]-acetonitrile $\delta_C = 1.24$, CD_2Cl_2 $\delta_C = 54.20$. Abbreviations used are s = singlet, d = doublet, dd = doublet or doublets, t = triplet, m = multiplet, br = broad. Elemental analyses (CHN) were carried out by the Analytische Laboratorien in Lindlar (Germany). Cyclic voltammetry measurements were performed with an Eco Chemie Autolab PGSTAT20. A conventional three-electrode cell, with Pt working and auxiliary electrodes and 0.1 M $[(Bu)_4N]PF_6$ (TBAH) electrolyte was used. An Ag/AgI reference electrode (grain of AgI, 0.02 M $[(Bu)_4N]I$ (TBAI) and 0.1 M TBAH) was employed. Experimental X-band EPR spectra were recorded on a Bruker ER220 spectrometer. The spectra were simulated by iteration of the anisotropic *g* values, (super)hyperfine coupling constants, the iridium nuclear quadrupole tensor, and line widths using XSophe EPR simulation software (Bruker BioSpin Corporation). The complexes $[\mathbf{1}]^+PF_6$[18] and $[Ir(coe)_2Cl]_2$[38] and the ligands Me_3tpa and Me_2tpa[39] were prepared according to literature procedures. All other chemicals are commercially available and were used without further purification, unless stated otherwise.

X-ray Diffraction. Selected bond lengths and angles are given in Tables 2, 4, and 5. Structure drawings are shown in Figures 2, 3, 4, 5, and 6. ORTEP drawings are shown in the Supporting Information (Figures S3-S10). Drawings were generated with the program PLATON.[40] Other relevant structure data are summarized in the Supporting Information.

DFT Geometry Optimizations and EPR Parameter Calculations. All geometry optimizations were carried out with the Turbomole program[41a] coupled to the PQS Baker optimizer.[42] Geometries were fully optimized as minima at the bp86[43] level using the Turbomole SV(P) basis set[41c,d] on all atoms (small-core pseudopotential[41c,e] on Ir). Improved energies were obtained from single-point calculations at the b3-lyp level[44] using the TZVP basis[41c,f] (small-core pseudopotential[41c,e] on Ir). EPR parameters[45] were calculated with the ADF[46] program system using the BP86[43] functional with the ZORA/V basis sets supplied with the program (triple-ζ plus two polarization functions on all atoms), using the coordinates from the X-ray structure as input (see Table 1). EPR parameter calculations using coordinates from a DFT optimized structure gave nearly identical results.

Synthesis of $[(Me_3tpa)Ir^{II}(\text{ethene})]^{2+}$ ($\mathbf{1}^{2+}$). 230 mg (0.33 mmol) of complex $[\mathbf{1}]^+PF_6$ was added to a solution of 86 mg (0.26 mmol) $[Fc]PF_6$ in 12 mL CH_2Cl_2. The resulting green/brown mixture was stirred for 30 min at room temperature. The resulting brown precipitate was collected by filtration. Yield 186 mg (0.221 mmol, 67%) $[\mathbf{1}]^{2+}(PF_6)_2$ (analytically pure). Deep brown/black crystals of $[\mathbf{1}]^{2+}(PF_6)_2$, suitable for X-ray diffraction, were obtained from a solution of the above precipitate in acetone, top-layered with hexane at 10 °C. Yield after crystallization: 72 mg (0.085 mmol, 33%). ESI$^+$−MS: m/z = 276.5 $[M-(PF_6)_2]^{2+}$, 698 $[M-PF_6]^+$. $\mu_{eff} = 2.22\mu_B$. Anal. Calcd for $C_{23}H_{28}N_4IrP_2F_{12}$: C 32.78, H 3.35, N 6.65; Found: C 32.64, H 3.33, N 6.67.

Synthesis of $[(Me_2tpa)Ir^{I}(\text{ethene})]^+$ ($\mathbf{2}^+$). $[Ir(coe)_2Cl]_2$ (266 mg, 0.2962 mmol) was dissolved in 9 mL methanol. Ethene was bubbled trough the solution until a clear solution was obtained. The solution was cooled to −30 °C and Me_2-tpa (191 mg, 0.998 mmol) was added under ethene. The reaction mixture was stirred until the ligand had dissolved. Subsequently, KPF_6 (157 mg, 0.853 mmol) was added and the solution was stirred for 1 h at −30 °C, after which the solution was cooled to −78 °C causing a yellow precipitate, which was collected by filtration and dissolved in 15 mL acetone. Nitrogen was bubbled trough the solution for 5 min. Subsequently, the solution was stirred

(38) Herde, J. L.; Lambert, J. C.; Senoff, C. V. *Inorg. Synth.* **1974**, *15*, 18.
(39) Nagao, H.; Komeda, N.; Mukaida, M.; Suzuki, M.; Tanaka, K. *Inorg. Chem.* **1996**, *35*, 6809−6815.
(40) Spek, A. L. PLATON, A Multipurpose Crystallographic Tool. Utrecht University, Utrecht, The Netherlands, **2003**.
(41) (a) Ahlrichs, R.; Bär, M.; Baron, H.-P.; Bauernschmitt, R.; Böcker, S.; Ehrig, M.; Eichkorn, K.; Elliott, S.; Furche, F.; Haase, F.; Häser, M.; Hättig, C.; Horn, H.; Huber, C.; Huniar, U.; Kattannek, M.; Köhn, A.; Kölmel, C.; Kollwitz, M.; May, K.; Ochsenfeld, C.; Öhm, H.; Schäfer, A.; Schneider, U.; Treutler, O.; Tsereteli, K.; Unterreiner, B.; von Arnim, M.; Weigend, F.; Weis, P.; Weiss, H. Turbomole Version 5, January 2002. Theoretical Chemistry Group, University of Karlsruhe; (b) Treutler, O.; Ahlrichs, R. *J. Chem. Phys.* **1995**, *102*, 346. (c) Turbomole basisset library, Turbomole Version 5, see (a); (d) Schäfer, A.; Horn, H.; Ahlrichs, R. *J. Chem. Phys.* **1992**, *97*, 2571. (e) Andrae, D.; Haeussermann, U.; Dolg, M.; Stoll, H.; Preuss, H. *Theor. Chim. Acta* **1990**, *77*, 123. (f) Schäfer, A.; Huber, C.; Ahlrichs, R. *J. Chem. Phys.* **1994**, *100*, 5829.
(42) (a) PQS version 2.4, **2001**, Parallel Quantum Solutions, Fayetteville, Arkansas, USA (the Baker optimizer is available separately from PQS upon request); (b) Baker, J. *J. Comput. Chem.* **1986**, *7*, 385.
(43) (a) Becke, A. D. *Phys. Rev. A* **1988**, *38*, 3089. (b) Perdew, J. P. *Phys. Rev. B* **1986**, *33*, 8822.
(44) (a) Lee, C.; Yang, W.; Parr, R. G. *Phys. Rev. B* **1988**, *37*, 785. (b) Becke, A. D. *J. Chem. Phys.* **1993**, *98*, 1372. (c) Becke, A. D. *J. Chem. Phys.* **1993**, *98*, 5648. (d) All calculations were performed using the Turbomole functional "b3-lyp", which is not identical to the Gaussian "B3LYP" functional.
(45) Lead reference for calculation of g-tensor (Zeeman interactions) parameters: van Lenthe, E.; van der Avoird, A.; Wormer, P. E. S. *J. Chem. Phys.* **1997**, *107*, 2488. Lead reference for calculation of A-tensor (Nuclear magnetic dipole hyperfine interactions) parameters: van Lenthe, E.; van der Avoird, A.; Wormer, P. E. S. *J. Chem. Phys.* **1998**, *108*, 4783.
(46) ADF2000.02. (a) Baerends, E. J.; Ellis, D. E.; Ros, P. *Chem. Phys.* **1973**, *2*, 41. (b) Versluis, L.; Ziegler, T.; *J. Chem. Phys.* **1988**, *88*, 322. (c) te Velde, G.; Baerends, E. J. *J. Comput. Phys.* **1992**, *99* (1), 84. (d) Fonseca Guerra, C.; Snijders, J. G.; te Velde, G.; Baerends, E. J. *Theor. Chem. Acc.* **1998**, *99*, 391.

for another 25 min, before it was added to 75 mL of hexane was added causing precipitation of [**2**]PF_6. The resulting orange solid was collected by filtration, washed 3 times with cold hexane and dried under vacuum (yield 217 mg, 54%). ^{1}H NMR (acetone-D_6, 298 K): δ 8.40 (1H, d, Py-H6); 7.75−7.05 (9H, Py−*H3*, Py−*H4* and Py−*H5*); 5.62−4.65 (6H, 6 × d[AB], N−CH_2−Py); 3.53 (s, 3H, Py−CH_3), 2.85 (s, 3H, Py−CH_3), 1.85 (m, 1H, CH_2═CH_2), 1.5−1.2 (m, 3H, CH_2═CH_2). ^{13}C NMR (CD_2Cl_2, 298 K): δ {165.4, 164.9, 164.0, 160.7, 160.3, 151.0, 137.2, 136.9, 135.5, 125.1, 125.0, 124.0, 122.2, 120.6, 119.4 (Py−C2, C3, C4, C5 and C6)}, {72.4, 70.4, 65.9 (N−CH_2−Py)}, {30.4, 27.8 (Py-CH_3)}, {4.04, 2.87 (CH_2═CH_2)}. Anal. Calcd for $C_{22}H_{26}N_4IrPF_6$: C 38.65, H 3.83 N 8.20; Found: C 38.56, H 3.86, N 8.08.

Synthesis of [(Me_2tpa)Ir^{II}(ethene)]$^{2+}$ (2^{2+}). Complex [**2**]$^{2+}$(PF_6)$_2$ was prepared similar to the procedure of [**1**]$^{2+}$(PF_6)$_2$, but using [**2**]$^+$-(PF_6) instead of [**1**]$^+$(PF_6). μ_{eff} = 1.84μ_B. Anal. Calcd for $C_{22}H_{26}N_4$-IrP_2F_{12}: C 31.89, H 3.16 N 6.76; Found: C 31.59, H 3.20, N 6.59.

Synthesis of [(Me^3tpa)Ir^{III}(MeCN)(C_2H_4)(Me_3tpa)Ir^{III}(MeCN)]$^{4+}$ (3^{4+}). 200 mg of [**1**]$^{2+}$(PF_6)$_2$ was dissolved in 10 mL acetonitril. The brown solution was stirred for 6 h in which time quantitatively a yellow solution of **3**$^{4+}$ was obtained. Layering of the solution with methanol yields transparent crystals. ^{1}H NMR (300 MHz CD_3CN, 298 K): δ 7.9−7.1 (18H, Py−H^3, Py−H^4 and Py−H^5), 4.78 (4H, d[AB], 16.4 Hz, N−CH_2−Py), 4.55 (4H, d[AB], 16.4 Hz, N−CH_2−Py), 4.54 (4H, s, N−CH_2−Py), 3.02 (6H, s, Py−CH_3), 2.72 (s, 6H, IrNC−CH_3), 2.68 (12H, s, Py−CH_3), 2.17 (4H, s, Ir−CH_2−CH_2−Ir). ^{13}C NMR (75 MHz CD_3CN, 298 K): δ 165.5 (Py^B−C^6), 163.8 (Py^B−C^2), 162.5 (Py^A−C^2), 157.5 (Py^A−C^6), 140.6 (Py^B−C^4), 140.1 (Py^A−C^4), 128.3 (Py^B−C^5), 127.5 (Py^A−C^5), 122.0 (Py^B−C^3), 120.4 (Py^A−C^3), 74.4 (Py^A−CH_2−N), 70.7 (Py^B−CH_2−N), 27.1 (Py^B−CH_3), 26.7 (Py^A−CH_3), 5.03 (NCCH_3), 3.05 (Ir−CH_2CH_2−Ir). The NCCH_3 signal is obscured by the solvent signal. Anal. Calcd for $C_{48}H_{59}N_{11}Ir_2$ P_4F_{24}: C 32.62, H 3.78 N 8.62; Found: C 33.54, H 3.47, N 8.68.

Synthesis of *R,R*-[(Me_2tpa)Ir^{III}(MeCN)(C_2H_4)(Me_2tpa)Ir^{III}-(MeCN)]$^{4+}$ (4a^{4+}) and *R,S*-[(Me^2tpa)Ir^{III}(MeCN)(C_2H_4)(Me_2tpa)Ir^{III}-(MeCN)]$^{4+}$ (4b^{4+}). 200 mg of [**1**]$^{2+}$(PF_6)$_2$ was dissolved in 10 mL acetonitril. An immediate color change from brown to yellow was observed as a 1:1 mixture of [**4a**]$^{4+}$(PF_6)$_4$ and [**4b**]$^{4+}$(PF_6)$_4$ was quantitatively obtained. Colorless crystals were obtained by layering the solution with methanol. NMR signals of **4a**$^{4+}$ partially overlap with those of **4b**$^{4+}$, but separated signals for Py−*H6*, Py−*Me*, Ir−NCCH_3 and Ir−CH_2CH_2−Ir fragments clearly reveal the presence of **4a**$^{4+}$ in equimolar amounts to **4b**$^{4+}$. Data for **4b**$^{4+}$: ^{1}H NMR (300 MHz, CD_3-CN, 298 K): δ 8.45 (2H, d, Py−H^6); 7.94−7.16 (18H, Py−H^3, Py−H^4 and Py−H^5); 4.85−4.30 (12H, six [AB]-type doublets, N−CH_2−Py); 2.92 (s, 6H, Py−CH_3), 2.78 (s, 6H, Py−CH_3), 2.71 (s, 6H, IrNC−CH_3), 1.68 (2H, m, AA′BB′, Ir−CH_2CH_2−Ir), 1.55 (2H, m, AA′BB′, Ir−CH_2CH_2−Ir). ^{13}C NMR (75 MHz, CD_3CN, 298 K): δ 165.3 (Py^B−C^6), 164.2 (Py^B−C^2), 162.9 (Py^A−C^2), 162.3 (Py^C−C^2), 157.6 (Py^A−C^6), 150.9 (Py^C−C^6), 140.8 (Py^B−C^4/ Py^C−C^4), 140.7 (Py^B−C^4/ Py^C−C^4), 140.4 (Py^A−C^4), 127.6 (Py^B−C,^{5} Py^C−C^5), 127.2 (Py^A−C^5), 124.5 (Py^C−C^3), 122.7 (Py^B−C^3), 120.5 (Py^A−C^3), 75.0 (Py^A−CH_2−N), 70.6 (Py$^{B/C}$−CH_2−N), 70.4 (Py$^{B/C}$−CH_2−N), 27.9 (Py^B−CH_3), 26.7 (Py^A−CH_3), 5.26 (NCCH_3), 4.98 (Ir−CH_2CH_2−Ir). The NCCH_3 signal is obscured by the solvent signal. Anal. Calcd for $C_{46}H_{54}N_{10}Ir_2P_4F_{24}$: C 32.29, H 3.18 N 8.18; Found: C 32.11, H 3.24, N 8.12.

Synthesis of *R,R*-[(Me_2tpa)Ir^{III}(Cl)(C_2H_4)(Me_2tpa)Ir^{III}(Cl)]$^{2+}$ (5a^{2+}) and *R,S*-[(Me_2tpa)Ir^{III}(Cl)(C_2H_4)(Me_2tpa)Ir^{III}(Cl)]$^{2+}$ (5b^{2+}). To a solution of 100 mg of [**1**](PF_6)$_2$ in acetone-d_6 was added an excess of sodium chloride. An immediate color change from green/brown to yellow was observed, yielding a mixture of several products (yield **5**$^{2+}$: 5%) after evaporation of the solvent. A 2:5 mixture of the diastereoisomers **5a**$^{2+}$ and **5b**$^{2+}$ was crystallized from dichloromethane layered with methanol. **5b**$^{2+}$: ^{1}H NMR (300 MHz, acetone-d_6): δ = 8.95 (d, $^3J_{HH}$ = 5.7 Hz, 2H, Py−H^6); 7.7−7.0 (m, 18H, Py−H^3, Py−H,^{4} and Py−H^5); 5.71 (d, $^3J_{HH}$ = 15.21 Hz, 2H, N−CH_2−Py); 5.2−4.6 (m, 10H, N−CH_2−Py); 3.00 (s, 6H, Py−CH_3), 2.81 (s, 6H, Py−CH_3). The ethylene signals are obscured by the solvent.^{13}C NMR (75 MHz, acetone-d_6): δ = {166.3, 165.5, 164.0, 158.2, 149.9, 138.9, 138.5, 138.1, 126.7, 125.9, 125.0, 122.5, 121.0, 120.5 (Py−C2, C3, C4, C5 en, C6)}, {74.1, 71.5, 70.9 (N−CH_2−Py)}, {27.4, 26.0 (Py−CH_3)}, 5.96 (Ir−CH_2−CH_2−Ir).

Synthesis of [(Me_3-tpa)Ir^I(NO)]$^{2+}$ (6^{2+}). A solution of [**1**](PF_6)$_2$ (20 mg, 0.024 mmol) in acetone (3 mL) was cooled to −78 °C and subjected to an atmosphere of NO(g) at 1.5 bar for 15 min. During this time, the atmosphere was refreshed three times. The color of the reaction mixture changed from greenish black to dark brown. Nitrogen was blown over the solution for 5 min, and then all volatiles were removed in vacuo. ^{1}H NMR (300 MHz, acetone-d_6): δ = 8.17 (t, $^3J_{HH}$ = 7.8 Hz, 2H, Py^A−H4), 7.88 (t, $^3J_{HH}$ = 7.7 Hz, 1H, Py^B−H4), 7.77 (d, $^3J_{HH}$ = 7.8 Hz, 4H, Py^A−H3 & Py^A−H5), 7.57 (d, $^3J_{HH}$ = 7.5 Hz, 1H, Py^B−H3/Py^B−H5), 7.41 (d, $^3J_{HH}$ = 7.5 Hz, 1H, Py^B−H3/Py^B−H5), 6.23 (d[AB], $^2J_{HH}$ = 15.6 Hz, 2H, NCH_2Py^A), 5.59 (d[AB], $^2J_{HH}$ = 15.6 Hz, 2H, NCH_2Py^A), 5.29 (s, 2H, NCH_2Py^B), 3.75 (s, 3H, Py^B−Me), 3.17 (s, 6H, Py^A−Me). ^{13}C NMR (75 MHz, acetone-d_6): δ = 165.06 (Py^A−C2/Py^A−C6), 163.99 (Py^A−C2/Py^A−C6), 162.84 (Py^B−C2/Py^B−C6), 159.38 (Py^B−C2/Py^B−C6), 143.18 (Py^A−C4), 141.54 (Py^B−C4), 127.79 (Py^A−C3/Py^A−C5), 126.42 (Py^B−C3/Py^B−C5), 123.49 (Py^A−C3/Py^A−C5), 120.85 (Py^B−C3/Py^B−C5), 72.82 (NCH_2-Py^A), 69.07 (NCH_2Py^B), 33.33 (Py^A−Me/Py^B−Me), 29.34 (Py^A−Me/Py^B−Me). Elemental analysis calcd (%) for ([**6**](PF_6)$_2$)$_2$·acetone $C_{44}H_{78}N_{10}O_3P_4F_{24}Ir_2$: C 30.93, H 3.09, N 8.02; found: C 30.80, H 3.28, N 7.85.

Synthesis of [(Me_3tpa)Ir^{III}(MeCN)(TEMPO)]$^{2+}$ (7^{2+}). A flame-dried reaction vessel was charged with MeCN (6 mL), TEMPO (20 mg, 0.128 mmol), and 4 Å mol sieves. The contents were stirred for 1 h, then [**1**](PF_6)$_2$ (90 mg, 0.107 mmol) was added. Stirring was continued for 2 h. The solvent was evaporated and a ^{1}H NMR spectrum was recorded in MeCN-d_3. ^{1}H NMR (200 MHz, MeCN-d_3): δ = 7.82 (t, $^3J_{HH}$ = 7.7 Hz, 2H, Py^A−H4), 7.59 (t, $^3J_{HH}$ = 7.7 Hz, 1H, Py^B−H4), {7.47 (d, $^3J_{HH}$ = 7.5 Hz, 2H), 7.35−7.26 (m, 5H), 7.10 (d, $^3J_{HH}$ = 7.8 Hz, 1H): Py^A−H3, Py^A−H5, Py^B−H3, Py^B−H5}, 5.72 (d[AB], $^2J_{HH}$ = 14.9 Hz, 2H, NCH_2Py^A), 4.83 (s, 2H, NCH_2Py^B), 4.71 (d[AB], $^2J_{HH}$ = 14.9 Hz, 2H, NCH_2Py^A), 4.16 (s, varying intensity, unknown), 3.31 (s, 3H, Py^B−Me), 3.08 (s, 3H, Ir−NCMe), 2.88 (s, 6H, Py^A−Me), 1.96 (s residual MeCN), 1.40 (br s, 6H, TEMPO −CH_2−), {0.95 (s, 6H), 0.18 (s, 6H): TEMPO−Me).

Synthesis of [(Me_3tpa)Ir^{III}(NHCOCH_3)(TEMPO*H*)]$^{2+}$ (8^{2+}). A solution of TEMPO (17 mg, 0.109 mmol) in MeCN (5 mL) was added to solid [**1**](PF_6)$_2$ (76 mg, 0.090 mmol). After 1 min, two drops of dioxygen-free water were added, and the reaction mixture was stirred overnight. Next, the suspension formed was filtered through a short plug of diatomaceous earth (without taking precautions against moisture or air) and concentrated to dryness in vacuo. Yellow, rhombic crystals of [**8**](BPh_4)$_2$·MeOH could be grown from a concentrated solution of [**8**](PF_6)$_2$ by top-layering it with a dilute solution of $NaBPh_4$ in MeOH. ^{1}H NMR (300 MHz, MeCN-d_3): δ = 12.32 (s, 1H, O···HN), 7.78 (t, $^3J_{HH}$ = 7.7 Hz, 2H, Py^A−H4), 7.54 (t, $^3J_{HH}$ = 7.7 Hz, 1H, Py^B−H4), 7.43 (d, $^3J_{HH}$ = 7.2 Hz, 2H, Py^A−H3/Py^A−H5), 7.36 (bs, 1H, Ir−N*H*C-(═O)Me), 7.23 (d, $^3J_{HH}$ = 7.8 Hz, 2H, Py^A−H3/Py^A−H5), 7.13 (d, $^3J_{HH}$ = 7.8 Hz, 2H, Py^B−H3 & Py^B−H5), 5.46 (d[AB], $^2J_{HH}$ = 15.6 Hz, 2H, NCH_2Py^A axial, *pointing toward TEMPOH*), 4.84 (d[AB],$^2J_{HH}$ = 15.6 Hz, 2H, NCH_2Py^A), 4.80 (s, 2H, NCH_2Py^B), 4.17 (s, 0.2H, unknown), 3.22 (s, 3H, Py^{B}Me), 2.88 (s, 6H, Py^{A}Me), 2.37 (s, 3H, Ir−NHC(═O)*Me*), 1.96 (s, residual MeCN), 1.60 (br s, 4H, TEMPO*H*−H3 & TEMPO*H*−H5), 1.58 (br s, 1H, TEMPO*H*−H4^a/TEMPO*H*−H4^b), 1.39 (br s, 1H, TEMPO*H*−H4^a/TEMPO*H*−H4^b), 1.09 (s, 6H, TEMPO*H*−Me), 0.44 (s, 6H, TEMPO*H*−Me *pointing toward complex*); ^{13}C NMR (75 MHz, MeCN-d_3): δ = 181.74 (Ir−NH*C*(═O)Me), 166.74 (Py^A−C2/Py^A−C6), 165.89 (Py^B−C2/Py^B−C6), 165.37 (Py^A−C2/Py^A−C6), 164.13 (Py^B−C2/Py^B−C6), 141.11 (Py^A−C4), 140.28 (Py^B−C4), 129.56 (Py^B−C3/Py^B−C5), 128.45 (Py^A−C3/Py^A−C5), 122.26 (Py^A−C3/Py^A−C5), 120.27 (Py^B−C3/Py^B−C5), 72.26 (NCH_2Py^B), 69.98

(NCH_2Py^A), 66.40 (unknown), 39.29 (TEMPO*H*−C3), 28.02 (TEMPO*H*−Me[a] *pointing toward complex*), 27.85 (Ir−NHC(═O)*Me*), 25.85 (Py^B−Me), 25.38 (Py^A−Me), 21.34 (TEMPO*H*−Me[b]), 16.30 (TEMPO*H*−C4), 1.69 (unknown), peak of TEMPO*H*−C2 not visible. Elemental analysis calcd (%) for [**8**]$(BPh_4)_2$·MeOH, $C_{81}H_{91}N_6O_3B_2Ir$: C 68.98, H 6.50, N 5.96; found: C 68.82, H 6.42, N 6.14.

Acknowledgment. This work was supported by The Netherlands Organization for Scientific Research (NWO-CW). We thank Dr. Peter H.M. Budzelaar for helpful tips & tricks concerning the DFT calculations and Paul P.J. Schlebos for the 2D-NMR measurements.

Supporting Information Available: Additional information about EPR simulation of compound $\mathbf{1}^{2+}$. Details of the X-ray structure determinations, ORTEP drawings and X-ray crystallographic data in CIF format for the structures within this paper. This material is available free of charge via the Internet at http://pubs.acs.org.

JA0439470